Identifying Human Preview Control Behavior Using Subsystem Identification

Bentinck, Pieter Bas J.C.; Pool, Daan M.; van der El, Kasper; Hoagg, Jesse B.; Mulder, Max

DOI
10.1016/j.ifacol.2022.10.251

Publication date
2022

Document Version
Final published version

Published in
IFAC-PapersOnline

Available online at www.sciencedirect.com

ScienceDirect

IFAC PapersOnline CONFERENCE PAPER ARCHIVE

IFAC PapersOnLine 55-29 (2022) 172–177

Identifying Human Preview Control Behavior Using Subsystem Identification

Pieter-Bas J. C. Bentinck,* Daan M. Pool,*
Kasper van der El,* Jesse B. Hoagg and Max Mulder***

* *Control and Simulation, Faculty of Aerospace Engineering, TU Delft, 2629 HS, Delft, The Netherlands (e-mail: {d.m.pool, k.vanderel, m.mulder}@tudelft.nl).*

** *Department of Mechanical and Aerospace Engineering, University of Kentucky, Lexington (KY), USA (e-mail: jhoagg@engr.uky.edu).*

Abstract: Better understanding of manual control requires more research on human anticipatory feedforward behaviour. Recent advances include a human control model for preview tracking, and a subsystem identification (SSID) technique that uses a candidate pool approach to identify the human feedforward and feedback responses. This paper discusses the performance of the SSID method when estimating the preview control model parameters. Through simulations of a preview task with two controlled element dynamics, the SSID performance with different remnant noise levels and candidate pool densities is quantified. We demonstrate its successful application to the preview model and show that its performance deteriorates for higher noise levels. While the feedforward parameters are estimated accurately, the high-frequency compensatory feedback dynamics cannot be reliably determined. Future work focuses on alternative formulations for using SSID to estimate preview model parameters. Since in manual control the closed-loop magnitude decreases at higher frequencies, effects of manipulating the weightings of the closed-loop fitting cost values at these frequencies must be further analyzed.

Keywords: Modeling of HMS, Modeling of human performance

1. INTRODUCTION

While a thorough understanding of Human Operator (HO) feedback control behavior exists, as well as validated models for predicting this behavior (McRuer and Jex, 1967; Mulder et al., 2018), the complex combination of feedback and feedforward behavior that characterizes HOs' behavior in pursuit and *preview* tracking tasks is less well understood. Recently, Van der El et al. (2016) proposed a novel linear time-invariant model that can accurately explain and predict behavior in pursuit/preview tracking tasks. The model is based on McRuer and Jex (1967)'s '*precision model*', can be applied to a range of different tasks (Van der El et al., 2016, 2020) and uses intuitive and identifiable parameters, such as a human look-ahead time. Essential for the development of such valuable HO models are accurate and reliable identification techniques that enable explicit separation of human feedback and feedforward control contributions (Mulder et al., 2018).

Recently, Zhang and Hoagg (2016a) proposed a novel Sub-System IDentification (SSID) technique for estimating human feedback and feedforward control responses as different subsystems in an overall closed-loop system. SSID uses a frequency-domain estimate of the closed-loop dynamics and a candidate pool approach to separate the internal feedforward and feedback contributions. Since then, SSID has been extended to include estimation of time delays (Zhang et al., 2018; Mousavi et al., 2020) and assessed with increasing noise levels and varying candidate pool densities (Mousavi et al., 2020; Sheffler et al., 2019). SSID's advantages over existing 'instrumental variable' techniques (Van Paassen and Mulder, 1998; Van der El et al., 2016) are that it guarantees stability of the estimated system dynamics and does not require *two* independent forcing functions to identify both feedback and feedforward responses. The latter potentially allows for identifying human feedback/feedforward control in more realistic tasks than currently possible. Thus, investigating whether SSID accurately estimates the parameters of Van der El et al. (2016)'s preview model is an important step.

The aim of this paper is to modify the SSID technique from (Mousavi et al., 2020) so that it can be applied to Van der El et al. (2016)'s preview model and to evaluate its performance for different remnant noise levels (Van der El et al., 2019) and candidate pool densities. For this analysis, offline simulations with a previously identified HO preview model (Van der El et al., 2020) are used, to provide a 'ground truth' for identification performance assessment. Furthermore, SSID results are presented for preview tasks with two types of controlled element (CE) dynamics – i.e., single and double integrator dynamics – as the CE affects both HOs' feedback and feedforward behavior and remnant characteristics (Van der El et al., 2019).

2. FEEDFORWARD HUMAN CONTROL MODELS

2.1 The Preview Tracking Task

To identify HO control behavior in preview tracking tasks, different approaches have been taken (Ito and Ito, 1975;

10.1016/j.ifacol.2022.10.251

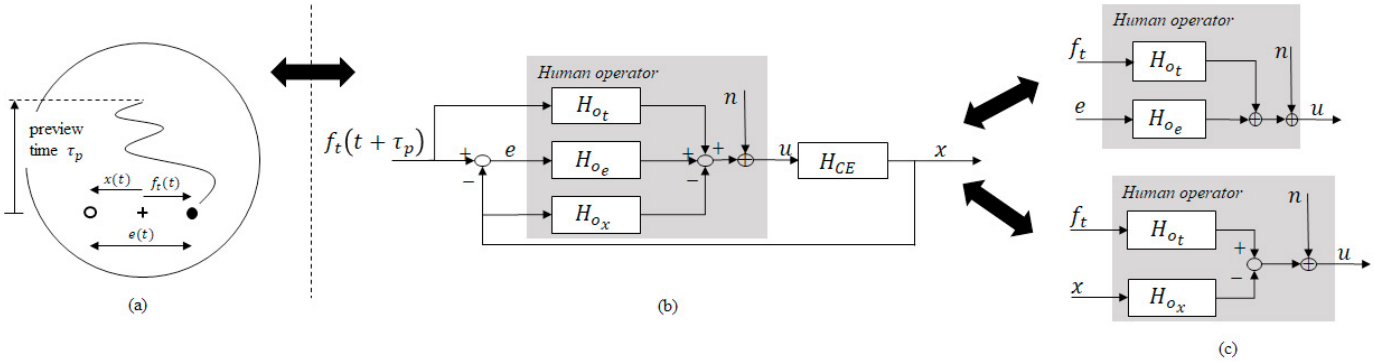

Fig. 1. Overview of a preview display (a), the three-channel block diagram that represents the human in a preview tracking task (b), and the two-channel simplifications (ET, top; TX, bottom) used for identification (c).

Van der El et al., 2016; Sheffler et al., 2019; Efremov et al., 2022). Fig. 1 shows the preview display and model structures used to describe HO behavior in preview tracking. Fig. 1(a) becomes a preview display when (part of) the future trajectory of f_t is shown; otherwise (i.e., for $\tau_p = 0$) it is a pursuit display. In a preview task, see Fig. 1(b), the human operator provides control outputs (u) to the CE, aiming to keep the CE output x (white circle in Fig. 1(a)) as close as possible to f_t (black circle), minimizing error e. Fig. 1(b) shows that in this task, HOs can respond to the target (f_t, feedforward), the error (e, feedback) and the CE output (x, feedback) presented on their display.

When identifying HO control dynamics in preview tasks, the three-channel control structure of Fig. 1(b) poses two key challenges: 1) it is an inherently overdetermined model structure, as the three inputs are not independent (i.e., $e = f_t - x$) and 2) most state-of-the-art identification techniques (e.g., (Van Paassen and Mulder, 1998)) require a separate independent forcing function for each estimated HO response. Therefore, the full model of Fig. 1(b) is often reduced to a two-channel model, where either the x or e responses are omitted, see Fig. 1(c). The resulting model structures are here referred to as ET (responses to e and f_t) and TX (f_t and x). Both two-channel model structures – which are equivalent and equally able to describe HO behavior – include the feedforward response that captures the feedforward behavior HOs use in preview tasks (Van der El et al., 2016).

All efforts to use SSID for the identification of human feedback and feedforward responses have used an ET model structure (Zhang and Hoagg, 2016a,b; Zhang et al., 2018; Sheffler et al., 2019). Many previous investigations into HO preview control behavior have also used the ET model structure (Ito and Ito, 1975; Efremov et al., 2022), however, Van der El et al. (2016)'s preview model (this paper) has a TX model structure.

2.2 Van der El's Preview Model

Van der El et al. (2016)'s preview model, see Fig. 2, is an extension of McRuer and Jex (1967)'s quasi-linear model for compensatory HO behavior. While generally identified using the TX structure of Fig. 1(c), its minimum realization has a '*prefiltered compensatory*' structure (Van der El et al., 2016). Fig. 2 shows that this implies that in preview tasks HOs minimize an 'internally calculated' error $e^\star$, based on the current CE output and a target $\tau_f \leq \tau_p$ seconds ahead, instead of the true error e.

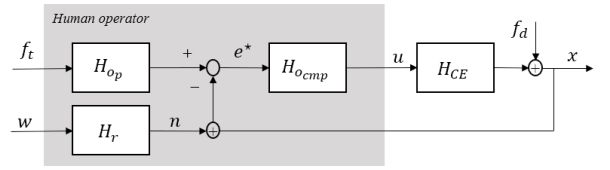

$$H_{o_{cmp}}(j\omega) = H_{o_{e^\star}} H_{nms} e^{-j\omega\tau_v}, \quad H_{o_{e^\star}}(j\omega) = K_e \frac{1+T_{L,e}j\omega}{1+T_{l,e}j\omega}, \quad H_{o_p}(j\omega) = H_{o_f} e^{j\omega\tau_f}$$

$$H_{o_f}(j\omega) = \frac{K_f}{T_{l,f}j\omega+1}, \quad H_{nms}(j\omega) = \frac{\omega_{nms}^2}{(j\omega)^2+2\zeta_{nms}\omega_{nms}(j\omega)+\omega_{nms}^2}, \quad H_r(j\omega) = \frac{K_r}{T_{l,r}j\omega+1}$$

K_f	= target response gain	τ_f	= look-ahead time
$T_{l,f}$	= lag/smoothing time-constant	K_e	= error response gain
$T_{L,e}$	= lead time-constant	$T_{l,e}$	= lag time-constant
ω_{nms}	= neuromuscular break frequency	τ_v	= time delay
ζ_{nms}	= neuromuscular damping ratio	K_r	= error response gain
$T_{l,r}$	= remnant lag time-constant		

Fig. 2. Van der El et al. (2016)'s HO preview model.

Fig. 2 shows that the prefilter dynamics H_{o_p} consist of the feedforward look-ahead time τ_f (a 'negative' delay) and a low-pass filter H_{o_f}, with a feedforward gain K_f and lag time constant $T_{l,f}$ as parameters. In this paper, the low-pass filter is rewritten to cut-off frequency form, i.e., with $\omega_{l,f} = 1/T_{l,f}$, for implementation in SSID (see Section 3). The compensatory dynamics $H_{o_{cmp}}$ are equivalent to those of traditional compensatory HO models (McRuer and Jex, 1967; Mulder et al., 2018) and consist of the equalization dynamics $H_{o_{e^\star}}$, the neuromuscular (NMS) dynamics H_{nms}, and a feedback time delay τ_v. The equalization dynamics vary with the type of CE dynamics (McRuer and Jex, 1967), as the lead time-constant $T_{L,e}$ is only non-zero for double integrator dynamics, while the lag-time constant is non-zero for gain dynamics only.

2.3 HO Remnant Model

In this paper we use Van der El et al. (2016)'s preview model as defined in Fig. 2 for generating representative data for identification tests with SSID. Besides the model itself, this requires also a simulation of the HO remnant n. As detailed in (Van der El et al., 2019) and shown in Fig. 2, our remnant model inserts the remnant signal, low-pass filtered Gaussian white noise, at the system output x. The remnant filter $H_r(j\omega) = K_r/(1+T_{l,r}j\omega)$ is parameterized with a gain K_r and a lag time-constant $T_{l,r}$, which both vary based on the CE dynamics (Van der El et al., 2019).

3. SUBSYSTEM IDENTIFICATION

3.1 The SSID Method

In this paper, we aim to estimate the parameters of Van der El et al. (2016)'s HO preview model using a modified version of the Subsystem Identification (SSID) technique in (Mousavi et al., 2020), which extends earlier work described in (Zhang and Hoagg, 2016a,b; Zhang et al., 2018). SSID estimates the dynamics of multiple subsystems (i.e., blocks) from a single measured 'overall' closed-loop input-output relation. The technique operates in the frequency domain and uses a candidate pool approach to ensure stability of the estimated system.

The central optimization objective of SSID is to find the parameter set Θ that minimizes the difference between a modelled closed-loop frequency response $H_{cl}^{mod}(j\omega_k)$ and a measured frequency response $H_{cl}^{meas}(j\omega_k)$. As also done in (Sheffler et al., 2019), here this is achieved by minimizing the cost function given by Eq. (1), which has the dependence on $j\omega_k$ omitted right of the equals sign for brevity. Note that Eq. (1) shows how $H_{cl}^{mod}(j\omega_k|\Theta)$ is related to the different control-loop subsystems shown in Fig. 2 and that no frequency-dependent weighting is applied. $H_{cl}^{meas}(j\omega_k)$ is estimated from the Fourier transforms of the input f_t and the output x, i.e., $H_{cl}^{meas}(j\omega_k) = X(j\omega_k)/F_t(j\omega_k)$.

$$J(\Theta) = \sum_{k=1}^{N_f} \left| \underbrace{\frac{H_{o_p}(\Theta)H_{o_{cmp}}(\Theta)H_{CE}}{1 + H_{CE}H_{o_{cmp}}(\Theta)}}_{H_{cl}^{mod}(\Theta)} - H_{cl}^{meas} \right|^2 \quad (1)$$

3.2 Changes for Preview Model Identification

The SSID implementation in this paper is modified with respect to (Mousavi et al., 2020) to allow for direct estimation of Van der El et al. (2016)'s model's parameters. Looking at Fig. 2, the subsystems that are to be identified are the prefilter dynamics H_{o_p} and the compensatory dynamics $H_{o_{cmp}}$. The modifications involve the following:

(1) *The model structure.* Instead of an ET model structure as used by Mousavi et al. (2020), a prefiltered compensatory model structure is used, see Fig. 2.
(2) *SSID's feedforward subsystem model.* Here, we use an infinite impulse response (IIR) model, as this enables the estimation of $\omega_{l,f}$. Mousavi et al. (2020) used a finite impulse response (FIR) feedforward model.
(3) *The coefficients of the closed-loop stability candidate pool.* This paper directly uses the preview model's coefficients to define the candidate pool, whereas this is mostly done using the transfer function coefficients.
(4) *No frequency weighting.* Mousavi et al. (2020) proposed frequency-dependent weights in the cost of Eq. (1). Here, all frequencies are weighted equally.

3.3 SSID Candidate Pool Definition

Fig. 3 shows an overview of the adapted SSID algorithm. In Step 1, the preview model's parameters (see Section 2) are divided over SSID's two candidate pools (CPs): the *closed-loop stability* CP Φ and the *feedforward time delay* CP Ψ. The closed-loop stability CP assures stability by only allowing parameter combinations that result in stable closed-loop poles. Non-CP model parameters – here only the prefilter gain $K_f\omega_{l,f}$, see Fig. 3 – are estimated directly as part of the optimization parameter vector α. In Step 2, the optimal value for the feedforward delay τ_f and the α parameters are found for each closed-loop stability CP (Φ) entry. This is done by minimizing the reduced cost function $\mathcal{Q}$ (Mousavi et al., 2020). Finally, Step 3 selects the final optimal parameters from all entries in the closed-loop stability CP, completing the estimation of Θ.

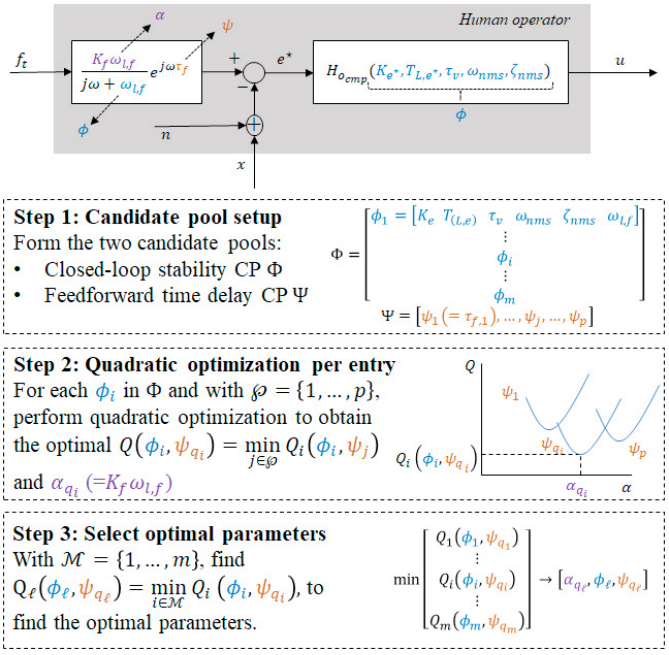

Fig. 3. Schematic overview of the SSID technique.

Following the methodology outlined by Sheffler et al. (2019) for dividing the different model parameters over the two CPs, H_{o_p} and $H_{o_{cmp}}$ are parameterized by their numerator and denominator coefficients; n_p, d_p, n_{cmp} and d_{cmp} are the respective numerator and denominator orders of N_{o_p}, D_{o_p}, $N_{o_{cmp}}$ and $D_{o_{cmp}}$. The coefficients of N_{o_p} are assigned to α, while all closed-loop stability coefficients D_{o_p}, $N_{o_{cmp}}$ and $D_{o_{cmp}}$ are collected in β. As indicated in Table 1, all α and β are expressed in terms of Van der El et al. (2016)'s HO model parameters. Furthermore, as the equalization dynamics $H_{o_{e^*}}$ (see Fig. 2) vary with the CE, the definition of β is different for the considered SI and DI cases. Also, it should be noted from Table 1 that $\omega_{l,f}$ occurs in both α and β; however, α only contains the product of K_f and $\omega_{l,f}$, which means that in fact only K_f is quadratically solved during Step 2.

4. METHOD: OFFLINE SIMULATIONS

4.1 Simulation Settings

HO model parameters In this paper, simulations are used to test SSID's performance for estimating the (known) HO model parameters, for different CP densities and remnant noise levels. Table 2 lists the HO model parameters based on Van der El et al. (2020)'s preview task with $\tau_p = 2$ s that were used to generate our simulated HO data.

Table 1. Subsystem order and α and β vector definitions for both CE dynamics.

	Subsystem Order				*HO Model Parameter Vectors*	
	n_p	d_p	n_{cmp}	d_{cmp}	α	β
SI	0	1	0	2	$\omega_{l,f}K_f$	$[\omega_{l,f} \quad \omega_{nms}^2 K_e \quad 2\zeta_{nms}\omega_{nms} \quad \omega_{nms}^2]$
DI	0	1	1	2	$\omega_{l,f}K_f$	$[\omega_{l,f} \quad \omega_{nms}^2 K_e T_{L,e} \quad \omega_{nms}^2 K_e \omega_{nms} \quad 2\zeta_{nms}\omega_{nms} \quad \omega_{nms}^2]$

Table 2. HO model simulation parameters and candidate pool limits and resolution.

HO parameter settings									
CE	H_{ce} [–]	$K_{e^\star}$ [-]	$T_{L,e^\star}$ [s]	τ_v [s]	ω_{nms} [rad/s]	ζ_{nms} [-]	K_f [-]	τ_f [s]	$T_{l,f}$ [s]
SI	$\frac{1.5}{(j\omega)}$	1.25	–	0.23	13.0	0.13	1.0	0.60	0.15
DI	$\frac{5}{(j\omega)^2}$	0.33	1.27	0.33	7.4	0.13	0.95	0.95	1.15
Candidate pool settings									
max		2	3	0.4	16	1	-	2	1.6
min		0.1	0.6	0.1	4	0.05	-	0.3	0
$n_{\theta,ref}$		6	3	3	4	2	-	3	2

Forcing Function Settings The target forcing function signals from Van der El et al. (2020)'s experiment were used. The f_t signals were sums of 10 sinusoids with a bandwidth (frequency after which amplitudes reduce 10x) of 1.5 rad/s, a measurement time of 120 s, and a standard deviation of 0.5 inch. For consistency with the experiment data (Van der El et al., 2020), five different f_t signals with different sinusoid phase realizations were used.

HO Remnant Settings As explained in Section 2.3, HO remnant is simulated as low-pass filtered Gaussian white noise. For SI and DI CE dynamics, the remnant time constant $T_{l,r}$ is respectively set to 12 s and 0.2 s (Van der El et al., 2019). The remnant gain K_f was determined iteratively to achieve a desired relative remnant level in the control output signal u, i.e., $\sigma_{u_n}^2/\sigma_u^2$. In this paper, we evaluate SSID's performance for different noise ratios (NRs) ranging from a no-remnant reference case to noise levels that exceed typical HO measurement data, i.e., $\sigma_{u_n}^2/\sigma_u^2 = 0$, 0.25, 0.5 and 0.75. All presented comparisons are based on 40 different remnant realizations. Consistent with experiment data processing of (Van der El et al., 2020), each simulation realization combines the frequency-averaged results from the five different f_t realizations.

4.2 SSID Settings

The main settings that need to be defined for SSID relate to its two candidate pools. The parameter ranges used here are listed in Table 2 and are based on results from previous experiments (Van der El et al., 2016, 2020). The same candidate pool settings (except for $T_{L,e^\star}$) were used for SI and DI dynamics. For each model parameter θ, a vector of candidate values was constructed based on the parameter limits, the CP density number d_{CP} and a tuned reference number of steps $n_{\theta,ref}$. The reference number of candidates for each parameter is shown in Table 2 and was selected based on a desired step size for $d_{CP} = 5$. For the analysis in this paper, we compared $d_{CP} = 1 - 5, 7, 10$ and 12, for which the number of candidates in the CP for each parameter can be calculated as $n_{\theta,ref}d_{CP}$. Based on all combinations of K_e, $T_{L,e}$, τ_v, ω_{nms}, ζ_{nms} and $T_{l,f}$, and filtering out those cases that result in unstable closed-loop system dynamics, the closed-loop stability CP Φ is constructed. In our implementation, the feedforward-delay CP Ψ contains all candidate τ_f values.

5. RESULTS

5.1 Cost Function

Fig. 4 shows the variation in the cost function of Eq. (1) for both CE dynamics for different d_{CP} settings and noise ratios (NRs). For noiseless data (NR = 0), J continues to reduce with increasing d_{CP}, especially for the SI data. This is expected, as with increased CP resolution the true parameter values can be approximated more accurately. For all NR > 0, the reduction in J with d_{CP} levels off for $d_{CP} > 5$ for both CE dynamics. This indicates that for realistic noisy HO data, at $d_{CP} = 5$ or higher increasing the CP density no longer helps to improve the fit to H_{cl}^{meas}. Comparing the results for SI and DI dynamics, the optimal J values for SI are more affected by remnant, with a larger discrepancy between the noiseless and noisy outcomes.

5.2 Parameter Estimates

Figs. 5 and 6 show the parameter estimates for $H_{o_{cmp}}$ and H_{o_p}, respectively. The graphs show the means (markers) and 95% confidence intervals (error bars) for the different noise levels for both CE dynamics. Furthermore, dashed lines indicate the true parameter value (black) and the parameter limits defined for the CP (red). For the parameters estimated using a CP, all CP candidates are shown as black crosses, while the gray shaded area highlights the two candidates closest to the true parameter value. For DI dynamics, the limits for K_e and τ_f were adjusted after $d_{CP} = 5$ to reduce computational time for the denser CPs. Figs. 5 and 6 show that this was allowed as the optimal fits, also at lower d_{CP} and with noise, did not occur in the excluded ranges. Note that the red CP limits and CP grid are not shown for K_f, as this parameter is estimated directly, see Section 3. Finally, all graphs have a second y-axis (right) that shows the percentage variation with respect to the true parameter value (Δ).

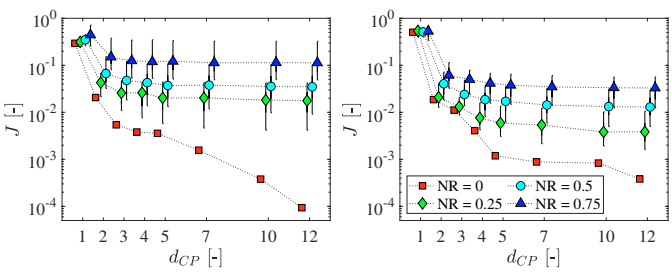

(a) SI (b) DI

Fig. 4. Cost function values for SI (a) and DI (b) for different noise levels and candidate pool densities.

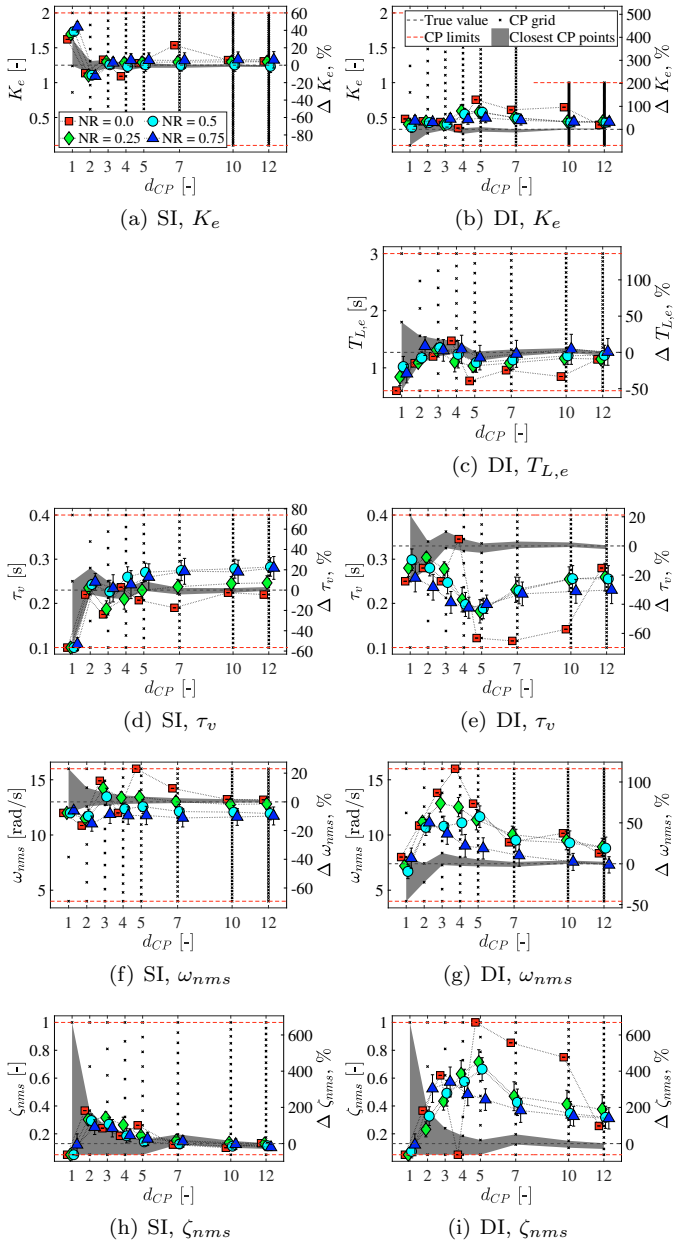

(a) SI, K_e (b) DI, K_e

(c) DI, $T_{L,e}$

(d) SI, τ_v (e) DI, τ_v

(f) SI, ω_{nms} (g) DI, ω_{nms}

(h) SI, ζ_{nms} (i) DI, ζ_{nms}

Fig. 5. Parameter estimates of the compensatory feedback subsystem $H_{o_{cmp}}$ for SI and DI CE dynamics.

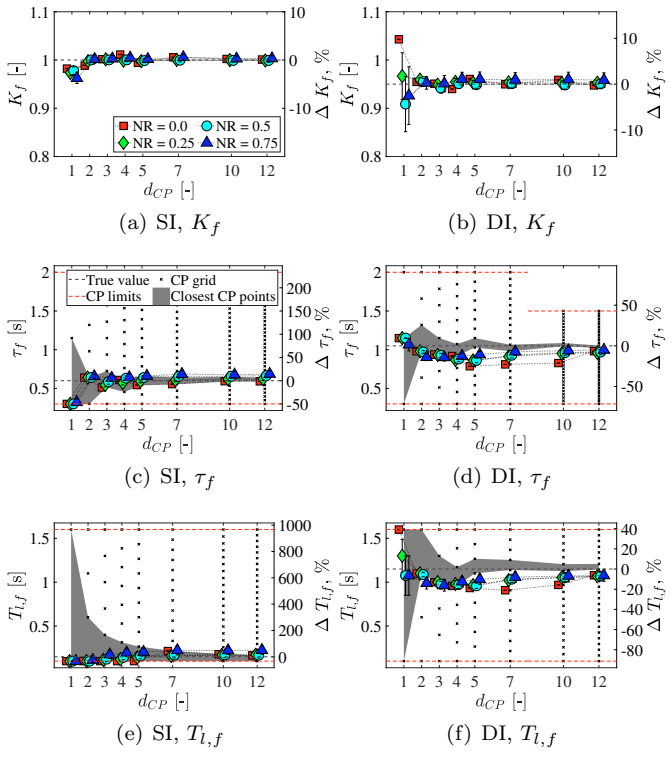

(a) SI, K_f (b) DI, K_f

(c) SI, τ_f (d) DI, τ_f

(e) SI, $T_{l,f}$ (f) DI, $T_{l,f}$

Fig. 6. Parameter estimates of the feedforward subsystem H_{o_p} for SI and DI CE dynamics.

Figs. 5 and 6 show that not all parameters are estimated with similar accuracy. For example, the prefilter gain K_f (Fig. 6(a) and 6(b)) shows an estimation error <1% for both dynamics and all NRs, while errors for the NMS damping ratio ζ_{nms} exceed 200% for DI dynamics, see Fig. 5(i). Also at high d_{CP}, where candidates much closer to the true parameter values are present in the CPs, these are not selected as SSID's optimal estimates. Overall, Figs. 5 and 6 show that H_{o_p}'s parameters and those parameters of $H_{o_{cmp}}$ that affect its low-frequency dynamics – K_e and $T_{L,e}$ – are estimated more accurately than those that characterize the high-frequency compensatory dynamics. This result is at least partly explained by the choice of cost function, i.e., Eq. (1); the magnitude of H_{cl} (SSID's fitting reference) in preview tracking tasks is much smaller at high frequencies (Van der El et al., 2020) (see also Fig. 7(a)), meaning also that high-frequency fitting errors may only have a minor influence on our SSID outcomes.

Furthermore, Figs. 5 and 6 show that both the estimation errors and the spread across different realizations are generally larger for DI than for SI dynamics. In terms of percentage error with respect to the true value (Δ), this is especially visible for K_e (33% vs. 2%), τ_v (22% vs. 14%), and ω_{nms} (27% vs. 4%). This effect is at least partly explained by the stronger influence of remnant for DI (Van der El et al., 2019). For some of the DI parameters the noiseless results are less accurate than those for NR > 0. This effect may be explained by our choice for an unweighted SSID cost (see Eq. (1)), which especially for the single NR = 0 data set results in many cost function minima with a similar J. Finally, the parameter estimates show that estimation biases reduce with increasing d_{CP}, also for $d_{CP} > 5$ when J no longer reduces, see Fig. 4. Looking at Figs. 5 and 6, $d_{CP} = 10$ is a good choice for both CEs and realistic NRs of 0.25-0.5.

5.3 Frequency Domain Fits

Fig. 7 shows example estimated closed-loop (H_{cl}) and subsystem (H_{o_p} and $H_{o_{cmp}}$) frequency response functions (FRFs) for noiseless DI data (NR = 0) and a selection of d_{CP} values. For SI and NR > 0 equivalent results were obtained, but these are not shown here for brevity. Fig. 7 shows that even with a low d_{CP} the closed-loop FRF (H_{cl}) is fitted accurately, especially at low frequencies, while the subsystem dynamics (H_{o_p} and $H_{o_{cmp}}$) are only approximated with much denser CPs, i.e., $d_{CP} = 10$. This is consistent with the parameter results in Figs. 5 and 6. Still, especially for $H_{o_{cmp}}$, even for high d_{CP} values

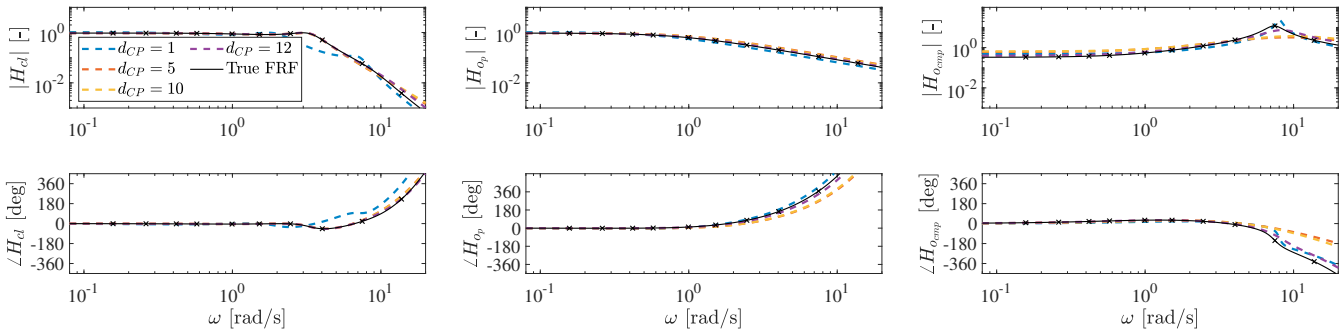

(a) Closed-loop H_{cl} (b) Prefilter H_{o_p} (c) Compensatory $H_{o_{comp}}$

Fig. 7. Frequency domain functions of the closed-loop (H_{cl}) and open-loop (H_{o_p} and $H_{o_{cmp}}$) of the estimated- and reference parameters for noiseless data for DI dynamics. Different lines indicate different CP densities.

high-frequency errors between the true FRFs and SSID estimates persist; normalized FRF fitting errors for the subsystem dynamics are found to be a factor 10-25 higher than those for H_{cl}. With the unweighted cost function of Eq. (1) and a magnitude of H_{cl} that is 10-100 times smaller above 3 rad/s (see also Fig. 7(a)), SSID is insufficiently sensitive to the high-frequency dynamics to accurately estimate all model parameters. However, the estimation accuracy may be improved by using a frequency-weighted SSID cost as proposed by Mousavi et al. (2020).

6. CONCLUSION

We investigated the application of a subsystem identification (SSID) technique to a recently proposed quasi-linear human operator model for preview tracking tasks. With some modifications it is shown how SSID can be successfully adapted to estimate the preview model parameters. Realistic operator model simulation data for two different controlled element dynamics, including remnant, were used to quantify how the estimation accuracy varied for different noise levels and SSID candidate pool densities. At realistic noise levels, a candidate pool density (d_{CP}) of 10 was found to be required to minimize both SSID's cost function and parameter estimation biases. While the human preview (prefilter) parameters were accurately estimated, the high-frequency compensatory feedback parameters (describing the neuromuscular system and time delay dynamics) showed errors of up to 200%. Future work includes a comparison of SSID's performance with other identification techniques, investigating alternative SSID candidate pool formulations for the preview model and study the effects of including frequency-dependent cost function weights to improve the SSID parameter estimation accuracy for higher frequency dynamics.

REFERENCES

Efremov, A.V., Tiaglik, M.S., and Irgaleev, I.K. (2022). Pilot Behavior Model in Pursuit and Preview Tracking Tasks. In *Proceedings of the AIAA SciTech Forum, San Diego (CA)*, AIAA-2022-0213.

Ito, K. and Ito, M. (1975). Tracking Behavior of Human Operators in Preview Control Systems. *Electrical Engineering in Japan*, 95(1), 120–127.

McRuer, D.T. and Jex, H.R. (1967). A Review of Quasi-Linear Pilot Models. *IEEE Trans. on Human Factors in Electronics*, HFE-8(3), 231–249.

Mousavi, S.A.S., Zhang, X., Seigler, T., and Hoagg, J.B. (2020). Subsystem identification of feedback and feedforward systems with time delay. *Results in Control and Optimization*, 1, 100002.

Mulder, M., Pool, D.M., Abbink, D.A., Boer, E.R., Zaal, P.M.T., Drop, F.M., Van der El, K., and Van Paassen, M.M. (2018). Manual Control Cybernetics: State-of-the-Art and Current Trends. *IEEE Trans. on Human-Machine Systems*, 48(5), 468–485.

Sheffler, A.J.S., Mousavi, S.A.S., Hellström, E., Jankovic, M., Santillo, M.A., Seigler, T.M., and Hoagg, J.B. (2019). Effects of Reference-Command Preview as Humans Learn to Control Dynamic Systems. In *IEEE Conf. on Syst., Man and Cyb.*, 4199–4204.

Van der El, K., Pool, D.M., Damveld, H.J., Van Paassen, M.M., and Mulder, M. (2016). An Empirical Human Controller Model for Preview Tracking Tasks. *IEEE Trans. on Cybernetics*, 46(11), 2609–2621.

Van der El, K., Pool, D.M., and Mulder, M. (2019). Analysis of Human Remnant in Pursuit and Preview Tracking Tasks. In *14th IFAC Symp. on Human-Machine Systems, Tallinn, Estonia*, 145–150.

Van der El, K., Pool, D.M., Van Paassen, M.M., and Mulder, M. (2020). Effects of Target Trajectory Bandwidth on Manual Control Behavior in Pursuit and Preview Tracking. *IEEE Trans. on Human-Machine Sys.*, 50(1).

Van Paassen, M.M. and Mulder, M. (1998). Identification of Human Operator Control Behaviour in Multiple-Loop Tracking Tasks. In *7th IFAC Symp. on Man-Machine Systems, Kyoto, Japan*, 515–520.

Zhang, X. and Hoagg, J.B. (2016a). Frequency-Domain Subsystem Identification with Application to Modeling Human Control Behavior. *Sys. & Contr. Letters*, 87.

Zhang, X. and Hoagg, J.B. (2016b). Subsystem Identification of Multivariable Feedback and Feedforward Systems. *Automatica*, 72, 131 – 137.

Zhang, X., Wang, S., Hoagg, J.B., and Seigler, T.M. (2018). The Roles of Feedback and Feedforward as Humans Learn to Control Unknown Dynamic Systems. *IEEE Trans. on Cybernetics*, 48(2), 543–555.